Remote Sensing of *Trichodesmium* spp. mats in the Western Tropical South Pacific

Guillaume Rousset[1], Florian De Boissieu[2], Christophe E. Menkes[3], Jérôme Lefèvre[4], Robert Frouin[5], Martine Rodier[6], Vincent Ridoux[7,8], Sophie Laran[7], Sophie Bonnet[9], and Cécile Dupouy[9]

[1]IRD (Institut de Recherche pour le Développement), UMR ESPACE DEV, Nouméa, New Caledonia
[2]IRSTEA, UMR TETIS, Montpellier, France
[3]IRD-Sorbonne Universités (UPMC, Université Paris 06)-CNRS-MNHN, Laboratoire d'Océanographie et du Climat: Expérimentations et Approches Numériques (LOCEAN), IRD Nouméa BP A5, 98848 Nouméa Cedex, New Caledonia
[4]LEGOS/MIO, 98800 Nouméa, New Caledonia
[5]Scripps Institution of Oceanography, University of California San Diego, La Jolla, CA 92093-0224, USA
[6]EIO (Ecosystèmes Insulaires Océaniens), Institut de Recherche pour le Développement-Université de la Polynésie Française-Institut Malarmé-Ifremer, Papeete, French Polynesia
[7]Observatoire Pelagis, UMS 3462, Université de la Rochelle/CNRS, La Rochelle, France
[8]Centre d'Etude de Chizé, UMR 7273 - CNRS- Université de La Rochelle, 2 rue Olympe de Gouges, 17000 La Rochelle, France
[9]Aix Marseille Université-CNRS-INSU, IRD, Mediterranean Institute of Oceanography (MIO), UM 110, IRD Nouméa, BP A5, 98848 Noumea Cedex, New Caledonia

Correspondence: Guillaume Rousset (guillaume.rousset@ird.fr)

Abstract. *Trichodesmium* is the major nitrogen-fixing species in the Western Tropical South Pacific (WTSP) region, a hotspot of diazotrophy. Due to the paucity of in situ observations, remote-sensing methods for detecting *Trichodesmium* presence on a large scale have been investigated to assess the regional-to-global impact of this organism on primary production and carbon cycling. A number of algorithms have been developed to identify *Trichodesmium* surface blooms from space, but determining with confidence their accuracy has been difficult, chiefly because of the scarcity of sea-truth information at time of satellite overpass. Here, we use a series of new cruises as well as airborne surveys over the WTSP to evaluate their ability to detect *Trichodesmium* surface blooms in the satellite imagery. The evaluation, performed on MODIS data at 250 m and 1 km resolution acquired over the region shows limitations due to spatial resolution, clouds, and atmospheric correction. A new satellite-based algorithm is designed to alleviate some of these limitations, by exploiting optimally spectral features in the atmospherically corrected reflectance at 531, 645, 678, 748, and 869 nm. This algorithm outperforms former ones near clouds, limiting false positive detection and allowing regional scale automation. Compared with observations, 80% of the detected mats are within a 2 km range, demonstrating the good statistical skill of the new algorithm. Application to MODIS imagery acquired during the February-March 2015 OUTPACE campaign reveals the presence of surface blooms Northwest and East of New Caledonia and near 20°S-172°W in qualitative agreement with measured nitrogen fixation rates. Improving *Trichodesmium* detection requires measuring ocean color at higher spectral and spatial (< 250 m) resolution than MODIS, taking into account environment properties (e.g., wind, sea surface temperature), fluorescence, and spatial structure of filaments, and a better

understanding of *Trichodesmium* dynamics, including aggregation processes to generate surface mats. Such sub-mesoscale aggregation processes for *Trichodesmium* are yet to be understood.

1   Introduction

The Western Tropical South Pacific (WTSP) is a Low Nutrient Low Chlorophyll (LNLC) region, harboring surface nitrate concentrations close to detection limits of standard analytical methods, and limiting for the growth of the majority of phytoplankton species (Le Borgne et al., 2011). This lack of inorganic nitrogen favors the growth of dinitrogen (N2)-fixing organisms (or diazotrophs), which have the ability to use the inexhaustible pool of N2 dissolved in seawater and convert it into bioavailable ammonia. Several studies have reported high N2 fixation rates in the WTSP (Berthelot et al., 2017; Bonnet et al., 2009, 2015; Garcia et al., 2007), which has recently been identified as a hot spot of N2 fixation (Bonnet et al., 2017). During austral summer conditions, N2 fixation supports nearly all new primary production and organic matter export (Caffin et al., 2018; Knapp et al., 2018) as nitrate diffusion across the thermocline and atmospheric sources of N are < 10% of new N inputs. The cyanobacterium *Trichodesmium* is one of the most abundant diazotrophs in our oceans (Capone, 1997; Luo et al., 2012) and in the WTSP in particular (Tenório et al., 2018; Stenegren et al., 2018). Cell-specific N2 fixation measurements recently conducted in the WTSP have revealed *Trichodesmium* as the major N2-fixing organism, accounting for > 60% of total N2 fixation (Bonnet et al., 2018). One of the characteristics of *Trichodesmium* is the presence of gas vesicles, which provide buoyancy (van Baalen and Brown, 1969; Villareal and Carpenter, 2003) and help maintain this cyanobacterium in the upper ocean surface. *Trichodesmium* cells are aggregated and form long chains called trichomes. Trichomes then can gather into colonies called "puffs" or "tuffs," and these colonies can aggregate at the surface of the water and form large mats that can extend for miles. They had already been observed during James Cook and Charles Darwin's expeditions. During the southern austral summer, *Trichodesmium* blooms have long been detected by satellite in the region, mostly around New Caledonia and Vanuatu (Dupouy et al., 2000, 2011), and later confirmed by microscopic enumerations (Shiozaki et al., 2014).

Identifying the occurrence and the spatial distribution of *Trichodesmium* blooms and mats is of primary importance to assess their regional contribution to primary production and biogeochemical cycles. However because of their paucity, scientific cruises alone are not sufficient to achieve such a goal, and remote sensing completed by sea observations of mats appear as the unique alternative for assessing its global impact. By using *Trichodesmium* spectral characteristics, among which pigment absorption due to phycoerythrin (PE) between 490 and 570 nm, absorption/scattering increase in the red-Near-Infrared (NIR), and particle backscattering (Subramaniam et al., 1999a, b; Hu et al., 2010), several empirical bio-optical algorithms have been developed to detect *Trichodesmium* blooms from various satellite sensors. They are extensively documented in Blondeau-Patissier et al. (2014) and Mckinna (2015). Former algorithms are classification schemes using thresholds applied to reflectances in the blue-green (440-550) range, like those proposed by Subramaniam et al. (2002) and Dupouy et al. (2011). They were designed using Sea-viewing Wide Field-of-view Sensor (SeaWiFS) observations. Using spectral features in Moderate Resolution Imaging Spectroradiometer (MODIS)-Aqua observations at 250 m in the red-NIR, McKinna et al. (2011) elaborated a simple reflectance classification algorithm to detect dense *Trichodesmium* surface aggregation. By providing an

operational Floating Algae Index (FAI), Hu et al. (2010) also demonstrated the potential for using the red-edge effect, that is the increasing absorption in the red (620-700) and scattering in the NIR (beyond 700) region of the spectrum due to floating algae. Using Medium Resolution Imaging Spectrometer (MERIS) observations in the red-NIR band, Gower et al. (2014) provided a similar index of *Trichodesmium* surface slicks. In their *Trichodesmium* bio-optical model, Westberry et al. (2005) used spe-

5   cific inherent optical properties (*Trichodesmium* specific absorption and backscattering parameters) to estimate *Trichodesmium* biomass from SeaWiFS reflectances.

The application of these algorithms to MODIS imagery revealed several issues, some of which were raised and discussed in the aforementioned articles. For example, the red-edge over *Trichodesmium* mats can lead to controversial results, since atmospheric correction for aerosols is based on information at similar wavelengths (Hu et al., 2010). Sampling effects are also

10   exacerbated due to the occurrence of clouds in the WTSP, since the blooming period of *Trichodesmium* (mainly November to March (Dupouy et al., 2011)) coincides with the cloudiest period of South Pacific Convergence Zone making difficult the identification of coincident in-situ mats in satellite imagery. Moreover, because *Trichodesmium* mats are narrow ($\backsim$ 50 m typically), the suitability of MODIS visible-NIR spatial resolution to detect such surface aggregations is questionable.

The aim of this study is to provide a systematic detection of *Trichodesmium* blooms in the vast WTSP Ocean between lati-

15   tudes 26° and 10°S and longitudes between 155° and 190° E, building on previously published algorithms and using marine reflectances measured by MODIS onboard Aqua. To evaluate the detection performance, a large database of historical mat observations in this region was created and updated with recent datasets and particularly the "Oligotrophy from Ultra-oligoTrophy PACific Experiment" (OUTPACE) cruise of March-April 2015 (Moutin et al., 2017). As a consequence of improvements in MODIS Collection 6 calibrations and algorithm updates for aerosol and cloud screening (Casey et al., 2017), *Trichodesmium*

20   detection algorithms developed with previous collections had to be adapted whenever possible. From this experience, a new algorithm less prone to contamination by clouds emerged, combining methods to detect *Trichodesmium* blooms from algorithms by McKinna et al. (2011) and Hu et al. (2010) and was evaluated using high resolution MODIS imagery. The paper is organized as follows. In Section 2 in-situ and satellite data used in this study are presented. In Section 3 methods to extract *Trichodesmium* spectral signature and their limitations are described, and details are provided about the former detection

25   algorithms of Hu et al. (2010) and McKinna et al. (2011), adapted for this study, as well as the newly developed algorithm. In Section 4 these algorithms are compared, and the proposed algorithm is evaluated along the OUTPACE cruise transect. In Section 5 the new algorithm performance is discussed. In Section 6 the conclusions of the study are drawn and perspectives are provided for future work.

2   Material

30   ### 2.1   In situ observations

The in-situ data used to train and test the *Trichodesmium* detection algorithm is a combination of three datasets, providing data in the acquisition period of MODIS Aqua or Terra missions (March 2000-present). The first dataset includes *Trichodesmium* mat observations published in Dupouy et al. (2011). These observations were made between 1998 and 2010, from aircraft,

French Navy ships, research vessels (e.g., R/V Alis), and ships of opportunity. Some of these visual observations were confirmed by water samples analyzed with photomicrographs confirming the abundant presence of *Trichodesmium* (Dupouy et al., 2011). The second dataset includes airborne visual observations were also gathered in December 2014 in the vicinity of New Caledonia during the "REcensement des Mammifères marins et autre Mégafaune pélagique par Observation Aérienne" (REM-MOA) program (Laran et al., 2016). This second dataset provides a large number of *Trichodesmium* mat observations along numerous and repetitive transects, which is most favorable for satellite data validation. In total, the database created from the compilation of these two datasets contains 507 open ocean observations in the region 15°S-25°S, 155°E-180°E (Figure 1). It is referred to as the Observation Base of *Trichodesmium* (OBT) in the following and used mainly for algorithm training.

A third dataset was obtained along a latitudinal transect around 20°S carried out during the OUTPACE scientific cruise (Moutin et al., 2017) in the region 160°E-160°W from 23 February to 01 April 2015. Seawater samples were collected for *Trichodesmium* identification and estimation by quantitative PCR, a molecular method described in Stenegren et al. (2018), microscopic counts at selected stations (Caffin, personal communication, 2017), as well as N2 fixation rates as described in Bonnet et al. (2018). Moreover, *Trichodesmium* abundance from the Underwater Vision Profiler 5 (UVP5; Picheral et al., 2010), calibrated on trichome concentration from pigment algorithms and on visual counts of surface samples at every stations, allowed one to describe the *Trichodesmium* distribution along the transect (Dupouy et al., 2018).

2.2 Satellite data

Marine reflectances from MODIS Aqua and Terra Collection 6 coinciding in time and space to the OBT database and the OUTPACE campaign are used in this study. Level-1A observations were downloaded from NASA's Goddard Space Flight Center (http://oceandata.sci.gsfc.nasa.gov) and processed with SeaDAS v7.0.2 to produce Level-2 reflectances at 250 m and 1 km resolution. SeaDAS v7.0.2 default values were applied during this processing for atmospheric correction failure, land, sun glint, very high or saturated radiance, sensor view zenith angle exceeding threshold, stray light contamination, and cloud contamination. Satellite observations with a proportion of valid pixels lower than 40% within the 0.5° searching radius around each in-situ observation were screened out.

MODIS atmospherically corrected (aerosol + Rayleigh) remote sensing reflectances (R_{rs}) in the visible, NIR, and short wavelength infrared (SWIR) were used at different resolutions: 250 m for bands 1 (645 nm) and 2 (859 nm), 500 m (bands 3-7, visible and SWIR land/clouds dedicated bands) and 1 km (bands 8-16). Bands 8 to 16 are dedicated to ocean color (Table 1), but the information in high-resolution bands located in the visible-NIR region is also used to track floating blooms. To evaluate the influence of resolution on detection performances, Level-2 remote sensing data was produced at both 250 m and 1 km resolutions, with interpolation of 500 m and 1 km data and aggregation of 250 m and 500 m resolution data, respectively. The consequences of these processing are discussed in Section 5.

The aerosol correction was carried out with the standard Gordon and Wang (1994) method since the study was conducted in the open ocean (Case-1 waters). For reasons detailed in next section, this type of correction is not appropriate in the presence of strong floating algae concentrations. Therefore, Rayleigh-corrected only reflectances (R_{rc}) were computed in addition to R_{rs} in Level-2 outputs.

3 Methods

3.1 Motivation in using Rayleigh-corrected reflectance (R_{rc}) in bio-optic algorithms for floating blooms

The atmospheric correction scheme of Gordon and Wang (1994) utilizes a pair of NIR bands at 748 and 869 nm. Spectral differences in the two NIR bands are used to select the most probable aerosol model, allowing an estimation of the aerosol effects in the visible. The aerosol contamination is then removed from the TOA signal after Rayleigh scattering correction to yield water-leaving radiance, therefore R_{rs}, in the visible. But to retrieve the aerosol model over Case-1 waters, the Gordon and Wang (1994) method relies on the assumption that optical constituents have negligible contribution to water-leaving radiances in the NIR region. Over floating mats, this assumption does not hold due to red edge effects, and the atmospheric correction may give erroneous (i.e., too low and even negative) values of R_{rs} as detailed in Hu et al. (2010). For this reason, R_{rc} was preferred in floating algal bloom concentration detection algorithms, as done with the Floating Algal Index (FAI) in Hu et al. (2010) or with the Maximum Chlorophyll Index (MCI) in Gower et al. (2008).

This issue is illustrated in Figure 2, which presents a MODIS-Aqua image of the Australian coast acquired just after a period of heavy rain that led to a massive *Trichodesmium* bloom. Fortunately, this bloom was also documented through field studies (McKinna et al., 2011). Figure 2A shows the "true-color" image obtained using a combination of R_{rc} at 469, 555 and 645 nm. On this image, large visible *Trichodesmium* mats distributed over a vast area can be seen. Figure 2B displays the SeaDAS-derived aerosol optical thickness (AOT) at 555 nm, an indicator of the aerosol load in the atmosphere. The high AOT values match the filamentous spatial structure noticed in the "true color" image. However, this structure is more likely to be floating material as the patterns are very thin and do not seem to be driven by wind. Moreover, several patches within this structure are flagged as cloud in the center (grey patches on figure 2B), although the "true color" image does not indicate the presence of clouds in this particular area. The misclassification of marine to cloudy pixel is a failure of the cloud detection algorithm, resulting from high water-leaving signal in the NIR bands exceeding the albedo threshold of 2.7% (Wang and Shi, 2005). Figure 2C shows the chlorophyll concentration (Chl_a) estimated according to the OC3 algorithm when Chl_a retrievals are above 0.2 $mg.m^{-3}$ and to the OCI algorithm when they are below (Hu et al., 2012). Chl_a decreases systematically, even falling to zero, in the vicinity of the *Trichodesmium* patches, although the real concentrations are certainly larger at the core of the mats than at their periphery. In addition to biomass underestimation, the spectral miscorrection may reduce the performance of reflectance classification schemes, like those based on simple reflectance thresholds or using reflectance ratios in the blue-green range. Prior to using such classification schemes, the spectral signature of *Trichodesmium* mats using MODIS R_{rs} and R_{rc} need to be further investigated (see below).

3.2 Extraction of the spectral signature of mats

With the persistent cloud cover in the region, the number of strict coincidences of in-situ observations and cloud-free MODIS pixels with visible *Trichodesmium* mats is small. To extract the *Trichodesmium* spectral signature corresponding to the OBT, 6 tiles have been specifically selected (Table 2) and are used later on to test the different bio-optical algorithms designed to detect the *Trichodesmium* presence. These images have been chosen because they are relatively free of clouds, *Trichodesmium*

mats are visible in the "true color" images, and they contain many "ground-truth" observations (Figure 3).

The NASA Ocean Biology Processing Group method (Bailey and Werdell, 2006) to select match-ups, i.e., average or nearest pixel, was used to find coincidences between in situ observations and clear MODIS satellite pixels. A total of 468 coincident MODIS Aqua pixels and OBT observations were found. After data screening, only 50 pairs remained, indicating that approx-

5   imately 90% of in-situ observations were not usable, primarily because of cloud cover. Once inspected, 19 MODIS-Aqua spectra out of the 50 pixels exhibited *Trichodesmium* features similar to those documented in Hu et al. (2010) and McKinna et al. (2011). In order to increase the number of useful observations, the searching window was extended both in time (up to +/- 4 days), with the hypothesis that a bloom can last for ⌣one week (e.g., Hegde et al., 2008), and extend spatially over +/- 50 km, i.e., ⌣200 pixels at 250 m resolution. This spatial relaxation up to +/- 50km is motivated by considering a maximum drifting

10   speed of ⌣ $10\ cm.s^{-1}$ for algae mats compatible with the observed surface surface drifts in that region (Rousselet et al., 2018; Cravatte et al., 2015). Also, some in-situ observations close spatially and temporarily (in the same tile and at intervals of +/- 4 days) increased our degree of confidence in identifying the filamentous patterns as due to *Trichodesmium*.

After extending the searching window, a total of 1200 spectra were extracted. Spectra were labelled, based on information provided by FAI (Hu, 2009) and the presence/absence of visible mats in the "true color" image. When the pixel is coinciding

15   with a visible mat on the "true color" image and is characterized with high FAI but low Chl_a, it is labeled Type i: it is the signature of high algae concentration. Pixels in close proximity to *Trichodesmium* mats with low FAI and undetected mats in "true color" image are labeled Type ii. This second type of pixels is expected to have a high amount of *Trichodesmium* colonies although not aggregated, offering an opportunity to detect spectral features due to the presence of *Trichodesmium* pigments other than Chl_a.

20   **3.3   Robust spectral features over and near *Trichodesmium* mats**

Figure 4B shows Type i average R_{rc} spectrum for 1km resolution images. Compared to blue water spectrum (see blue curve) no *Trichodesmium* spectral feature could be detected in the visible and NIR spectral domain. The increase of R_{rc} beyond 700 nm indicates that, at low resolution, the red edge effect is weakly discernible over floating algae, contrasting with robust signals detected by McKinna et al. (2011) and Hu et al. (2010) using both hyperspectral and MODIS 250x250 m observations

25   over *Trichodesmium* mats. As suggested by these authors, spectral sensors with 1 km resolution are inappropriate to capture floating *Trichodesmium* due to negligible signal from discrete mats once mixed with adjacent water in 1x1 km cells. Middle and bottom rows of Figure 4 present R_{rc} and R_{rs} spectra interpolated to 250 m and partitioned in Type i and Type ii (second row and third row respectively). For Type i, it is noteworthy that the red edge signal is well captured in the NIR region at 859 nm, a MODIS land band with true 250 m resolution , while in the 758 and 896 nm bands the derived signals using bilinear

30   interpolation are still low. One can notice that, after application of the NIR atmospheric correction, the shape of the mean R_{rs} spectra remains similar to that of R_{rc}, minus an offset in the visible region, corresponding to subtraction of the flawed aerosol contribution (compare Figure 4C with Figure 4D). Derived R_{rs} at 748 and 869 nm are set to zero, as a result of the black pixel approximation.

For Type ii, the red-edge effect totally disappears from the true 250 m band at 859 nm and the derived baseline 758-869 nm

appears above the R_{rc} (and R_{rs}) at 859 nm. Hu (2009) had already noticed this issue for pixels with strong spatial gradients in the NIR part of the spectrum. It is interpreted as a result of the bilinear interpolation of 758 and 869 nm bands from 1 km to 250 m, using information from adjacent 1 km pixels.

Unfortunately, in the visible region, there is little useful information to capture *Trichodesmium* with R_{rc} (or R_{rs}) spectra

5 interpolated to 250 m, both in Type i and Type ii situations. In *Trichodesmium* blooms, a release of dissolved colored substance was observed, as suggested by Hu et al. (2010) for coastal waters. For oligotrophic waters studied here, there was no such absorption in the blue region (412 nm) due to possible dissolved colored substances. Other characteristic features due to absorption maxima around 495 and 550 nm caused by the presence of phycourobilin and phycoerythrobilin respectively (see Figure 5 in Hu et al. (2010)), are not seen using the 600 spectra-composite spectrum. Finally, the only robust spectral feature

10 in the visible range is a minimum in R_{rc} (and R_{rs}) occurring at 678 nm, due to increasing reflectance beyond 700 nm.

Interestingly, comparison between R_{rc} and R_{rs} shows that standard deviation error bars are much smaller for R_{rc} reflectances while the range of magnitudes between wavelengths is larger. This is a significant argument for using R_{rc} instead of R_{rs}, as it would lead to a better discrimination of *Trichodesmium* mat spectra against other spectra.

3.4 Two published algorithms

15 Among the existing *Trichodesmium* mat detection algorithms, only the McKinna et al. (2011) and Hu et al. (2010) ones were designed for the MODIS sensor and were tested in this study. The other algorithms were ignored as they were not adaptable to MODIS sensor or would give erroneous results due to Chl_a misestimation over *Trichodesmium* mats.

The *Trichodesmium* mat detection algorithm of McKinna et al. (2011) is based on 4 criteria relative to the shape of R_{rs} (given in te Appendix A). When applied to the same MODIS image (new collection) as the one used by McKinna et al.

20 (2011), more pixels were discarded due to the fourth criterion, which eliminated pixels whith negative nLw at 555, 645, 678 or 859 nm). Indeed, the test of a negative R_{rs} value at 678 nm due to aerosol overcorrection excludes many pixels. Other atmospheric corrections including that of Wang and Shi (2007) used by McKinna et al. (2011), have been applied with the same results. Skipping the fourth criterion of the algorithm allowed matching the results of McKinna et al. (2011). Therefore, this modification was adopted for the present study and the algorithm is called "McKinna modified" in the following.

25 The *Trichodesmium* detection algorithm presented in Hu et al. (2010) is based on a two-step analysis of R_{rc} spectra. The first step captures floating algae with FAI. The second step resolves the ambiguities between *Trichodesmium* and *Sargassum*, by analyzing spectral features in the blue-green region. To overcome possible spectral influence due to inappropriate atmospheric correction, Hu et al. (2010) proposed a simple correction method based on the difference of R_{rc} spectra between bloom and nearby algae free region. After several tries on the data presented above, the second step was found to be sensitive to the choice

30 of the algae free region (not shown). Thus, the detection was made only by applying thresholds on FAI. After tuning, best results were obtained when FAI was between 0 and 0.04.

3.5 New algorithm criteria

Our criteria for detecting *Trichodesmium* mats were defined based on spectral characteristics of R_{rs} and R_{rc} (Figure 4). Similarly to the algorithms of Hu et al. (2010) and McKinna et al. (2011) (see Appendix), three criteria given in equations 1-3 were defined to extract the typical spectrum shape of *Trichodesmium*. The first criterium (Eq. 1) takes advantage of the systematic negative R_{rs} values at 678 nm over strong *Trichodesmium* mat concentrations. All pixels with negative R_{rs} value at this wavelength have a high probability to be floating algae and thus *Trichodesmium* in this region. Moreover, this criterium has been found useful can also be used to detect some artifact, e.g., sun glint.

The second criterium (Eq. 2) is based on $R_{rc}(748)$ and $R_{rc}(859)$ to detect the spectral shape in the NIR associated with the surface *Trichodesmium* mats. The third criterium (Eq. 3) uses $R_{rc}(645)$ and $R_{rc}(531)$ to resolve ambiguities between *Trichodesmium* mats and incorrectly selected pixels after processing with the previous criteria, the misdetections occurring mostly near clouds (Eq. 3).

$$R_{rs}(678) < 0 \tag{1}$$
$$R_{rc}(748) < R_{rc}(859) \tag{2}$$
$$R_{rc}(645) < R_{rc}(531) \tag{3}$$

4 Results

4.1 Comparison with previous algorithms

The detection results of the three *Trichodesmium* detection algorithms are illustrated in Figure 5 on the MODIS tile A2007290.0355, used in McKinna et al. (2011). The McKinna modified algorithm shows the same detection patterns as the ones found in McKinna et al. (2011). It is a vast *Trichodesmium* area within which the filamentous structures cannot be distinguished. The new algorithm and the threshold FAI detect thin filamentous structures more similar to *Trichodesmium* mat structures observed in airborne photographs. When negative, the absolute value of $R_{rs}(678)$ can also be used as an index of mats concentration as values increase when getting to the core of patches.

Compared with both former algorithms, the new algorithm performs much better near clouds. Figure 6 is a zoom of the area delineated by the red rectangle in Figure 5. This area presents a cloud patch where McKinna modified and FAI algorithms both detect *Trichodesmium* pixels. These pixels were identified as false positives as their spatial distribution is sparse and only in the vicinity of clouds. This conclusion is also supported by the "true color" composition (Figure 2) where the only *Trichodesmium* mats appear located at the bottom of the image. In that area the new algorithm does not make any false positive detection while keeping the *Trichodesmium* mats at the bottom of the image. The robustness of the new detection algorithm to exclude cloud-contaminated pixels while keeping accurate *Trichodesmium* mat detection is an important improvement for regions with high cloudiness, such as the WTSP.

4.2 Algorithm performance against in-situ mat observations

The exact coincidence in time and space between in-situ *Trichodesmium* mats observations and satellite mat detection is quite difficult to reach in general. One of the main reasons is by far the cloud cover, which eliminates a large quantity of the possible comparisons (90%). A second reason is the elapsed time between in-situ observations and the corresponding satellite pass during which the floating algae could have drifted at sea surface and/or migrated vertically depending on sea conditions (temperature, wind, etc.). For example, the abundance of *Trichodesmium* at the sea surface may vary with the time of day, as a daily cycle of rising and sinking colonies in the water column is often observed as a result of cell ballasting (Villareal and Carpenter, 2003). Moreover, as *Trichodesmium* is a buoyant constituent, it can be advected by surface currents.

To circumvent that problem and perform a more statistically robust comparison of the detection results of our algorithm with in-situ data, we used the following strategy. An analysis of the spatio-temporal distance between the in-situ observations and the nearest detected mats was conducted. As explained previously, for each day in a range of +/- 4 days around the date of observation, the spatial distance between the position of the observation and the nearest detected mat was computed. Overall, 80% of the observed mats have a corresponding mat detection within less than 5 km range independent of the detection algorithm used. These results demonstrate the statistical capability of the new algorithm to retrieve a mat near a point of observation.

4.3 Algorithm application for the OUTPACE cruise

The new algorithm was applied to MODIS data acquired during the OUTPACE cruise time. A total of 140 tiles at 250 m resolution covered the time period February 15 - April 7, 2015 and the spatial area of the cruise. Due to high cloud cover during the cruise, only a few tiles were exploitable. *Trichodesmium* mats were detected from 12 MODIS-Aqua and 3 MODIS-Terra tiles. Figure 7B shows the detected mats over these tiles (in blue). Note that the OUTPACE cruise actually crossed a number of *Trichodesmium* satellite detections. In order to further illustrate the results, a crude qualitative presence/absence scheme was applied to better visualize which OUTPACE stations were coincident with the algorithm positive detection. We selected areas within 50 km of each OUTPACE station and labeled the station as presence when there was at least one pixel detected as positive in the satellite algorithm. In figure 7B, the red points indicate presence and blue points absence.

Trichodesmium mats were mostly observed visually northeast of New Caledonia one week before the cruise and during the first days of the cruise (on board observation) by video and photographs. No other mats were observed during the rest of the cruise, but there was not any dedicated observer that would actually permit such visual observation, unlike during the (REMMOA) campaigns. Nevertheless, Underwater Vision Profiler 5 (UVP5) counts of colonies and phycoerythrin and trichome concentrations along the transect show that *Trichodesmium* contribution was maximum in the Melanesian Archipelago, i.e., the Western part of the transect, where slicks are numerous, and then fairly well related to *Trichodesmium* concentrations in the upper layer (Dupouy et al., 2018). The other high spot of mats detected in the satellite imagery is at LDB (station name in OUTPACE), where no slick was observed but where *Trichodesmium* was in high concentration, although mixed with a high abundance of picoplanktonic cyanobacteria (Dupouy et al., 2018).

Bonnet et al. (2018) reported a significant (p<0.05) correlation between N2 fixation rates and *Trichodesmium* abundances during OUTPACE. Based on bulk and cell-specific N2-based isotopic measurements indicated that *Trichodesmium* accounted for 50 to >80% of N2 fixation rates in this region at the time of the cruise. Such a high correlation between *Trichodesmium* biomass (here phycoerythrin) was also measured in New-Caledonia waters (Tenório et al., 2018). Hence the in situ N2 fixation rate measured during the cruise (Figure 7A) was used as a robust proxy of the *Trichodesmium* concentration to further evaluate accuracy of satellite detections. A qualitative comparison between Figures 7A and 7B indicates that when significant fixation rates were observed, *Trichodesmium* presence was detected by the satellite algorithm and when N2 fixation rates were low, *Trichodesmium* absence was stated. Although qualitative, this successful validation gives confidence in using our algorithm for *Trichodesmium* detection.

5 Discussion

5.1 Algorithm limitations

The proposed algorithm was designed to detect strong concentrations of floating *Trichodesmium* mats and limit wrong detections. However, floating *Trichodesmium* mats are occurring when sea surface is little agitated since they tend to sink and disperse in rough conditions. In such a case our algorithm does not allow to detect *Trichodesmium* even in strong concentration because of the low penetration depth of NIR irradiance (below 1 m). This situation occurred during the OUTPACE cruise, where measurements reveal high *Trichodesmium* abundances near the Fiji island (Stenegren et al., 2018), while our algorithm was unable to detect *Trichodesmium* mats (Figure 7, stations adjacent 180°E).

Another limitation concerns the validity of the new algorithm for future MODIS collections and other regions. The first criterion is taking advantage of the aerosol overcorrection as an index of floating algae. The aerosol correction algorithm will certainly be adapted in the future. Thus, first criterion would have to be replaced by another floating algae index; the FAI could be a good solution. However, it will always be possible to use the current (imperfect) aerosol correction. Moreover, the zero threshold on $R_{rs}(678)$, under which the pixel is labelled as a Trichodesmium mat, would have to be tested and tuned in other situations, e.g., in the presence of aerosols and other floating material. This study was carried out in the WTSP area, where the observed spectra seem slightly different from the ones reported in McKinna et al. (2011) and Hu et al. (2010). More specifically, the spectral oscillations of reflectance observed by Hu et al. (2010) in the range [412, 678] nm were not noticed in the present study. Therefore, the robustness of this algorithm in the presence of other floating algae (e.g., *Sargassum*), as well as in other regions of the world, would have to be tested to make it more general.

This study was limited to the processing of MODIS images, mainly because of the availability of images corresponding to field measurements (2014 and before). However, it would be worth extending the detection algorithm to other sensors such as MERIS, e.g., for comparison with the Gower et al. (2014) algorithm, and the recently launched Ocean and Land Colour Instrument (OLCI). This would require further investigations to adapt the algorithm to the specific bands of these sensors and evaluate the results. However, since these sensors cover the same spectral range, one can expect a quite similar behavior.

Aware of these limitations, one may consider using R_{rc} only, since R_{rs} is sensitive to the accuracy of the atmospheric correction. To emulate an index of mats concentration, Equation (4) is proposed in place of Equation (1). The magnitude of the trough at 678 nm is an indication of the mats concentration, which can be retrieved using the difference between the observed $R_{rc}(678)$ and the result of the linear R_{rc} interpolation between 645 and 748 nm. In the following, To confirm the trough at 678 nm, check the spectral form typical to *Trichodesmium* (Figure 4), and assess the red-edge of the signal, equations (5-7), similar to the form criteria of McKinna et al. (2011), could be used:

$$[(R_{rc}(645) + (R_{rc}(748) - R_{rc}(645)) \times \frac{678 - 645}{748 - 645}] - R_{rc}(678) > 0 \qquad (4)$$

$$R_{rc}(678) < R_{rc}(859) \qquad (5)$$

$$R_{rc}(678) < R_{rc}(748) \qquad (6)$$

$$R_{rc}(678) < R_{rc}(667) \qquad (7)$$

This alternative algorithm has the advantage of being easily adaptable to other sensors with similar spectral bands (e.g. MODIS). Moreover, the procedure is free of atmospheric overcorrection while still exploiting the red-edge effect. However in its application, a large part of pixels detected as *Trichodesmium* by the former algorithm (i.e., described in Section 3.5) is discarded. The different criteria cannot be relaxed without a false positive detection increase. Therefore this alternative algorithm is more restrictive, and its suitability and performance require further examination.

5.2   Spatial resolution impact

As indicated previously, only few spectral bands (land channels) have a high resolution (250 m or 500 m), while the rest have a nominal resolution at 1 km. To investigate the influence of resolution on the spectral signature of *Trichodesmium* mats the spectral analysis was also conducted at a 1 km resolution. Dense groups of extended mats are still well detected at 1 km resolution. However, thinner mats with a weaker signal visible at 250 m resolution are lost at 1 km resolution. Figure 8 illustrates this behavior on MODIS data.

The spatial structure of *Trichodesmium* aggregates is complex. When mats are present, *Trichodesmium* have a tendency to form a filamentous pattern much narrower than 250 m (50 m at most, according to visual detections), and thus the satellite sensor at 250 m resolution can only detect the largest ones (Figures 8 and 9). Hence there is a scale mismatch between the exact form of the thin filaments and the actual detection by the current satellite data, which must average in a way the thin and strongest filaments into signals detectable at 250 m. Understanding the shape of the filaments, and their physical characteristics (e.g., width) will require much higher resolution satellite data (at least 50 m) which are available at present but without repetitive coverage. Figure 9 additionally illustrates that the *Trichodesmium* filaments are but a tiny part of the chlorophyll tongues and are inserted into the much wider chlorophyll patterns. There can exist, within a chlorophyll tongue such as that in Figure 9, several thin elongated filaments.

One would also intuitively believe that the filaments illustrate the presence of dynamical fronts where convergent dynamics can maintain and participate in the mat aggregations. A natural dynamical criteria allowing one to characterize the presence

of the filaments could be found in the finite-size Lyapunov exponents (FSLE) methods (Rousselet et al., 2018). A relationship between FSLE only and in situ chlorophyll edges "fronts" was found during OUTPACE with a 25% correlation score. The same kind of relationship was expected for floating algae filaments. However, the relationship between FSLE and the organisation of the filaments could not be proven within this study. We believe that it is here also a question of scale. The present calculation of FSLE is using 12.5 km satellite data at best (Rousselet et al., 2018), thus it is difficult to think that such a resolution could catch dynamics Trichodesmium filaments wide of a few hundred meters. A dedicated in situ experiments would have to be specifically undertaken to resolve the question of filament organization.

6 Conclusions and perspectives

At present, previously published algorithms detecting *Trichodesmium* using the current MODIS data archive (Hu et al., 2010; McKinna et al., 2011), cannot be directly used in the South Pacific as they either miss the mats due to algorithms failures (Section 3.4) and/or do not eliminate numerous false positive in the presence of clouds. In our study, we have devised a new algorithm building on the previous ones, which allows a cleaner and more robust detection of those mats. Validation was accomplished using a new, updated database of mats in the South Pacific. This algorithm can however detect only the densest slick but achieves the goal of limiting the detection of false positive due to clouds. During the OUTPACE cruise, satellite detections confirmed the presence of *Trichodesmium* slicks at much wider spatial range than what was possible to observe from the ship. This illustrates the important contribution and complementary nature of satellite observations to in situ measurements. Yet, the new detection algorithm was developed and evaluated for the WTSP region. Hence, future prospects will be to extend the evaluation to other regions, especially in the presence of other floating algae such as *Sargassum*.

During the same campaign Dupouy et al. (2018) found that ocean color measured with a Satlantic UV-VIS radiometer at greenish blue and yellowish green wavelengths were not totally linked to Chl_a and that an extra factor independent of Chl_a, may be related to colony backscattering or fluorescence, governs part of the variability. This extra factor is not observed during BIOSOPE (Biogeochemistry and Optics South Pacific Experiment), a cruise in the tropical Southern Pacific gyre (Claustre et al., 2008), where the radiance is correlated to Chl_a only. Further investigations have to be conducted to confirm that such a signal is produced by *Trichodesmium* and can be detected from space.

MODIS-Terra and MODIS-Aqua satellite sensors are acquiring data since 2000 and 2002, respectively. However, the data quality of these sensors is becoming more and more uncertain with time going by, as their lifetime was not expected to last more than 6 years. The new algorithm could be adapted to other satellite instruments with similar spectral bands, for example Visible Infrared Imaging Radiometer Suite (VIIRS) onboard NPP and JPSS-1/NOAA-20 (1 km resolution) and OLCI onboard Sentinel-3 (300 m spatial sampling), but the spatial resolution remains a problem as we observed that 250 m was already too coarse a resolution to understand the thinner mat dynamics. A study with a better spectral and spatial resolution may lead to better performances and to a new and better algorithm. It may be possible, at least regarding spatial resolution, with Multispectral Instrument (MSI) onboard the Sentinel-2 series (10 to 60 m resolution).

It has previously been documented that near dense *Trichodesmium* mats some satellite products like the satellite chlorophyll concentration are inaccurate. In order to better constrain the contribution of *Trichodesmium* to nitrogen and carbon biogeochemical cycles, this algorithm must be corrected. Using R_{rc} instead of R_{rs} is possible (section 5.1), but some adjustments and comparisons with in-situ measurements must first be carried out. Globally such algorithm would allow one to estimate the

5 *Trichodesmium* amount aggregated in sea surface mats. The next step is to understand the quantitative aspect linking the *Trichodesmium* abundances to N2 fixation rates, including their vertical distribution even when *Trichodesmium* filaments/colonies are spread out in the water column. Another important field of interest is to be able to understand phytoplankton functional types using satellites including *Trichodesmium* (de Boissieu et al., 2014). At present, we do not know any such study that included *Trichodesmium* but we have hopes that with our new in situ database and our understanding of the mat shapes detected

10 in the present study, and the development of performing statistical methods such as machine learning, advances can be made in that regard, a perspective for future work.

Finally Dutheil et al. (2018) explore the regional and seasonal budget of the N2 fixation due to *Trichodesmium* in a numerical model based on physical and biogeochemical properties that does not take into consideration the spatial characteristic of *Trichodesmium* colonies to aggregate in mats. One interesting aspect will be to find a way to integrate our results in such model

15 to better estimate the regional effects of that species.

Appendix A: McKinna et al. (2011) algorithm

The McKinna et al. (2011) algorithm is based on the analysis of the above-water reflectance spectrum of a moderate *Trichodesmium* mat, similar to the one measured on colonies in a small dish with an Ocean Optics spectroradiometer (Dupouy et al., 2008). It uses typical spectral characteristics of the normalized water-leaving radiance (nLw) after atmospheric correc-

20 tion to define 4 *Trichodesmium* detection criteria. The first three criteria relate to the shape of the spectrum and the last criteria discards any pixel with negative nLw. When these 4 criteria are respected the pixel is identified as revealing the presence of *Trichodesmium*:

$$nLw(859) > c1.nLw(678) \tag{A1}$$
$$nLw(645) > nLw(678) \tag{A2}$$
25 $$nLw(555) > nLw(678) \tag{A3}$$
$$nLw(555), nLw(645), nLw(678), nLw(859) < 0 \tag{A4}$$

Appendix B: Hu et al. (2010) algorithm

The detection algorithm, originally developed by (Hu, 2009) for floating algae can be applied to *Trichodesmium* mats, as demonstrated by Hu et al. (2010) on MODIS-Aqua images of the west coast of Florida and the Gulf of Mexico, even though

30 the *Trichodesmium* mats occurred in Case 2 waters. This algorithm can be decomposed into two steps: 1) detection of floating

algae (FAI, Floating Algal Index), and 2) test-of-form criteria of the radiance spectrum.

The FAI aims at detecting the strong reflectance in the infrared (red-edge) of the algal agglomerate. To avoid the atmospheric overcorrection linked to the red-edge effect of the floating algae organized in a heap (Hu, 2009), the calculation of this index is applied to reflectance corrected only for the effects of Rayleigh scattering (R_{rc}). This correction accounts for the major part of the color of the atmosphere if aerosols are not too abundant (i.e., small optical thickness). The FAI is then defined as the difference between R_{rc} in the infrared (859 nm for MODIS) and a reference reflectance ($R_{rc,0}$) calculated by linear interpolation between the red and shortwave infrared, i.e., 667 nm and 1240 nm for MODIS:

$$R_{rc,NIR} + (R_{rc,SWIR} - R_{rc,RED}) \times \frac{\lambda_{NIR} - \lambda_{RED}}{\lambda_{SWIR} - \lambda_{RED}} \tag{B1}$$

$$\lambda_{RED} = 645nm, \lambda_{NIR} = 859nm, \lambda_{SWIR} = 1240nm \tag{B2}$$

where RED = 645 nm, NIR = 859 nm, and SWIR = 1240 nm. According to Hu et al. (2010), the difference between R_{rc} and $R_{rc,0}$ (the second term of Equation B1) allows one to deal with the majority of the atmospheric effect which has a quasi-linear spectral shape between 667nm and 1240nm. The second step of the algorithm consists in identifying the mats emphasized by the FAI thanks to the shape of the spectrum in the visible domain. So as to correct the bias inferred in the visible part of the spectrum by the possible presence of mats, Hu et al. (2010) suggest applying to the pixels presenting a strong FAI value the correction of an area situated immediately next to this pixel and without bloom. This approach being very computer expensive, it is substituted by a simple difference between the R_{rc} spectrum of the pixels considered (i.e., eventually with *Trichodesmium*) and that of a nearby zone without mat. The spectrum of this R_{rc} difference presents a pattern (spectral signature) that seems to be specific to *Trichodesmium* presence, i.e., a succession of high type low-top-low-top for the wavelengths 469-488-531-551-555 nm.

Competing interests. no competing interests are present

Acknowledgements. R. Frouin is supported by the National Aeronautics and Space Administration under various grants. We thank NASA for the MODIS products.

References

Bailey, S. W. and Werdell, P. J.: A multi-sensor approach for the on-orbit validation of ocean color satellite data products, Remote Sensing of Environment, 102, 12–23, https://doi.org/10.1016/j.rse.2006.01.015, 2006.

Berthelot, H., Benavides, M., Moisander P, H., Grosso, O., and Bonnet, S.: High-nitrogen fixation rates in the particulate and dissolved pools in the Western Tropical Pacific (Solomon and Bismarck Seas), Geophysical Research Letters, 44, 8414–8423, https://doi.org/10.1002/2017GL073856, 2017.

Blondeau-Patissier, D., Gower, J. F. R., Dekker, A. G., Phinn, S. R., and Brando, V. E.: A review of ocean color remote sensing methods and statistical techniques for the detection, mapping and analysis of phytoplankton blooms in coastal and open oceans, https://doi.org/10.1016/j.pocean.2013.12.008, 2014.

Bonnet, S., Biegala, I. C., Dutrieux, P., Slemons, L. O., and Capone, D. G.: Nitrogen fixation in the western equatorial Pacific: Rates, diazotrophic cyanobacterial size class distribution, and biogeochemical significance, Global Biogeochemical Cycles, 23, 1–13, https://doi.org/10.1029/2008GB003439, 2009.

Bonnet, S., Rodier, M., Turk-Kubo, K., Germineaud, C., Menkes, C., Ganachaud, A., Cravatte, S., Raimbault, P., Campbell, E., Quéroué, F., Sarthou, G., Desnues, A., Maes, C., and Eldin, G.: Contrasted geographical distribution of N2 fixation rates and nifH phylotypes in the Coral and Solomon Seas (southwestern Pacific) during austral winter conditions, Global Biogeochemical Cycles, 29, 1874–1892, https://doi.org/10.1002/2015GB005117, 2015.

Bonnet, S., Caffin, M., Berthelot, H., and Moutin, T.: Hot spot of N2 fixation in the western tropical South Pacific pleads for a spatial decoupling between N2 fixation and denitrification, Proceedings of the National Academy of Sciences, 114, E2800–E2801, https://doi.org/10.1073/pnas.1619514114, 2017.

Bonnet, S., Caffin, M., Berthelot, H., Grosso, O., Benavides, M., Helias-Nunige, S., Guieu, C., Stenegren, M., and Foster, R. A.: In depth characterization of diazotroph activity across the Western Tropical South Pacific hot spot of N2 fixation, Biogeosciences Discussions, pp. 1–30, https://doi.org/10.5194/bg-2017-567, 2018.

Caffin, M., Moutin, T., Foster, R. A., Bouruet-Aubertot, P., Doglioli, A. M., Berthelot, H., Guieu, C., Grosso, O., Helias-Nunige, S., Leblond, N., Gimenez, A., Petrenko, A. A., de Verneil, A., and Bonnet, S.: N$_{2}$ fixation as a dominant new N source in the western tropical South Pacific Ocean (OUTPACE cruise), Biogeosciences, 15, 2565–2585, https://doi.org/10.5194/bg-15-2565-2018, 2018.

Capone, D. G.: Trichodesmium, a Globally Significant Marine Cyanobacterium, 1997.

Casey, K. A., Polashenski, C. M., Chen, J., and Tedesco, M.: Impact of MODIS sensor calibration updates on Greenland Ice Sheet surface reflectance and albedo trends, The Cryosphere, 11, 1781–1795, https://doi.org/10.5194/tc-11-1781-2017, 2017.

Claustre, H., Sciandra, A., and Vaulot, D.: Introduction to the special section bio-optical and biogeochemical conditions in the South East Pacific in late 2004: the BIOSOPE program, Biogeosciences, 5, 679–691, https://doi.org/10.5194/bg-5-679-2008, 2008.

Cravatte, S., Kestenare, E., Eldin, G., Ganachaud, A., Lefèvre, J., Marin, F., Menkes, C., and Aucan, J.: Regional circulation around New Caledonia from two decades of observations, Journal of Marine Systems, 148, 249–271, https://doi.org/https://doi.org/10.1016/j.jmarsys.2015.03.004, 2015.

de Boissieu, F., Menkes, C., Dupouy, C., Rodier, M., Bonnet, S., Mangeas, M., and Frouin, R. J.: Phytoplankton global mapping from space with a support vector machine algorithm, in: Ocean Remote Sensing and Monitoring from Space, edited by Frouin, R. J., Pan, D., and Murakami, H., https://doi.org/10.1117/12.2083730, 2014.

Dupouy, C., Jacques, N., Subramaniam, A., R. Mulholland, M., Montoya, J., Campbell, L., and et D. Capone, E.: Satellite captures Trichodesmium blooms in the Soutwestern Tropical Pacific, Eos Transactions American Geophysical Union, 81, 13, 2000.

Dupouy, C., Neveux, J., Dirberg, G., Röttgers, R., Barboza Tenório, M. M., and Ouillon, S.: Bio-optical properties of the marine cyanobacteria Trichodesmium spp., Journal of Applied Remote Sensing, 2, 023 503, https://doi.org/10.1117/1.2839036, 2008.

5 Dupouy, C., Benielli-Gary, D., Neveux, J., Dandonneau, Y., and Westberry, T. K.: An algorithm for detecting Trichodesmium surface blooms in the South Western Tropical Pacific, Biogeosciences, 8, 3631–3647, 2011.

Dupouy, C., Frouin, R., Tedetti, M., Maillard, M., Rodier, M., Lombard, F., Guidi, L., Picheral, M., Duhamel, S., Charrière, B., and Sempéré, R.: Diazotrophic \textit{Trichodesmium} influence on ocean color and pigment composition in the South West tropical Pacific, Biogeosciences Discussions, pp. 1–43, https://doi.org/10.5194/bg-2017-570, 2018.

10 Dutheil, C., Aumont, O., Gorguès, T., Lorrain, A., Bonnet, S., Rodier, M., Dupouy, C., Shiozaki, T., and Menkes, C.: Modelling the processes driving \textit{Trichodesmium} sp. spatial distribution and biogeochemical impact in the tropical Pacific Ocean, Biogeosciences Discussions, pp. 1–34, https://doi.org/10.5194/bg-2017-559, 2018.

Garcia, N., Raimbault, P., and Sandroni, V.: Seasonal nitrogen fixation and primary production in the Southwest Pacific: Nanoplankton diazotrophy and transfer of nitrogen to picoplankton organisms, Marine Ecology Progress Series, 343, 25–33,
15 https://doi.org/10.3354/meps06882, 2007.

Gordon, H. R. and Wang, M.: Retrieval of water-leaving radiance and aerosol optical thickness over the oceans with SeaWiFS: a preliminary algorithm, Appl. Opt., 33, 443–452, https://doi.org/10.1364/AO.33.000443, 1994.

Gower, J., King, S., and Goncalves, P.: Global monitoring of plankton blooms using MERIS MCI, International Journal of Remote Sensing, 29, 6209–6216, https://doi.org/10.1080/01431160802178110, 2008.

20 Gower, J., King, S., and Young, E.: Global remote sensing of Trichodesmium, International Journal of Remote Sensing, 35, 5459–5466, https://doi.org/10.1080/01431161.2014.926422, 2014.

Hegde, S., Anil, A., Patil, J., Mitbavkar, S., Krishnamurthy, V., and V. Gopalakrishna, V.: Influence of environmental settings on the prevalence of Trichodesmium spp. in the Bay of Bengal, Marine Ecology Progress Series, 356, 2008.

Hu, C.: A novel ocean color index to detect floating algae in the global oceans, Remote Sensing of Environment, 113, 2118–2129,
25 https://doi.org/10.1016/j.rse.2009.05.012, 2009.

Hu, C., Cannizzaro, J., Carder, K. L., Muller-Karger, F. E., and Hardy, R.: Remote detection of Trichodesmium blooms in optically complex coastal waters: Examples with MODIS full-spectral data, Remote Sensing of Environment, 114, 2048–2058, 2010.

Hu, C., Lee, Z., and Franz, B.: Chlorophyll a algorithms for oligotrophic oceans: A novel approach based on three-band reflectance difference, Journal of Geophysical Research: Oceans, 117, 1–25, https://doi.org/10.1029/2011JC007395, 2012.

30 Knapp, A. N., McCabe, K. M., Grosso, O., Leblond, N., Moutin, T., and Bonnet, S.: Distribution and rates of nitrogen fixation in the western tropical South Pacific Ocean constrained by nitrogen isotope budgets, Biogeosciences, 15, 2619–2628, https://doi.org/10.5194/bg-15-2619-2018, 2018.

Laran, S., Hamani, V., Authier, M., Dorémus, G., Van Canneyt, O., Ridoux, V., and Watremez, P.: Distribution et abondance de la mégafaune marine dans le sud-ouest du Pacifique. Campagne REMMOA - Nouvelle-Calédonie et Wallis et Futuna, Rapport final pour l'Agence des
35 aires marines protégées,105pp, 2016.

Le Borgne, R., Allain, V., Griffithos, S. P., Matear, R. J., McKinnon, D. A., Richardson, A. J., and Young, J. W.: Vulnerability of open ocean food webs in the tropical Pacific to climate change, in: Vulnerability of tropical Pacific fisheries and aquaculture to climate change, pp. 189–249, SPC, http://www.documentation.ird.fr/hor/fdi:010058145, 2011.

Luo, Y.-W., Doney, S. C., Anderson, L. a., Benavides, M., Berman-Frank, I., Bode, a., Bonnet, S., Boström, K. H., Böttjer, D., Capone, D. G., Carpenter, E. J., Chen, Y. L., Church, M. J., Dore, J. E., Falcón, L. I., Fernández, a., Foster, R. a., Furuya, K., Gómez, F., Gundersen, K., Hynes, a. M., Karl, D. M., Kitajima, S., Langlois, R. J., LaRoche, J., Letelier, R. M., Marañón, E., McGillicuddy, D. J., Moisander, P. H., Moore, C. M., Mouriño-Carballido, B., Mulholland, M. R., Needoba, J. a., Orcutt, K. M., Poulton, a. J., Rahav, E., Raimbault, P., Rees, a. P., Riemann, L., Shiozaki, T., Subramaniam, a., Tyrrell, T., Turk-Kubo, K. a., Varela, M., Villareal, T. a., Webb, E. a., White, a. E., Wu, J., and Zehr, J. P.: Database of diazotrophs in global ocean: abundance, biomass and nitrogen fixation rates, Earth System Science Data, 4, 47–73, https://doi.org/10.5194/essd-4-47-2012, 2012.

McKinna, L., Furnas, M., and Ridd, P.: A simple, binary classification algorithm for the detection of Trichodesmium spp. within the Great Barrier Reef using MODIS imagery, Limnology and Oceanography: Methods, 9, 50–66, https://doi.org/10.4319/lom.2011.9.50, 2011.

Mckinna, L. I. W.: Three decades of ocean-color remote-sensing Trichodesmium spp . in the World's oceans : A review, Progress in Oceanography, 131, 177–199, https://doi.org/10.1016/j.pocean.2014.12.013, 2015.

Moutin, T., Doglioli, A. M., de Verneil, A., and Bonnet, S.: Preface: The Oligotrophy to the UlTra-oligotrophy PACific Experiment (OUT-PACE cruise, 18 February to 3 April 2015), Biogeosciences, 14, 3207–3220, https://doi.org/10.5194/bg-14-3207-2017, 2017.

Picheral, M., Guidi, L., Stemmann, L., Karl, D. M., Iddaoud, G., and Gorsky, G.: The Underwater Vision Profiler 5: An advanced instrument for high spatial resolution studies of particle size spectra and zooplankton, Limnology And Oceanography-methods, 8, 462–473, https://doi.org/10.4319/lom.2010.8.462, 2010.

Rousselet, L., de Verneil, A., Doglioli, A. M., Petrenko, A. A., Duhamel, S., Maes, C., and Blanke, B.: Large- to submesoscale surface circulation and its implications on biogeochemical/biological horizontal distributions during the OUTPACE cruise (southwest Pacific), Biogeosciences, 15, 2411–2431, https://doi.org/10.5194/bg-15-2411-2018, 2018.

Shiozaki, T., Kodama, T., and Furuya, K.: Large scale impact of the island mass effect through nitrogen fixation in the western South Pacific Ocean, Geophysical Research . . . , pp. 1–7, https://doi.org/10.1002/2014GL059835, 2014.

Stenegren, M., Caputo, A., Berg, C., Bonnet, S., and Foster, R. A.: Distribution and drivers of symbiotic and free-living diazotrophic cyanobacteria in the western tropical South Pacific, Biogeosciences, 15, 1559–1578, https://doi.org/10.5194/bg-15-1559-2018, 2018.

Subramaniam, A., Carpenter, E. J., and Falkowski, P. G.: Bio-optical properties of the marine diazotrophic cyanobacteria Trichodesmium spp. I. Absorption and photosynthetic action spectra, https://doi.org/10.4319/lo.1999.44.3.0618, 1999a.

Subramaniam, A., Carpenter, E. J., and Falkowski, P. G.: Bio-optical properties of the marine diazotrophic cyanobacteria Trichodesmium spp. II. A reflectance model for remote-sensing, https://doi.org/10.4319/lo.1999.44.3.0618, 1999b.

Subramaniam, A., Brown, C. W., Hood, R. R., Carpenter, E. J., and Capone, D. G.: Detecting Trichodesmium blooms in SeaWiFS imagery, Deep-Sea Research Part II: Topical Studies in Oceanography, 49, 107–121, 2002.

Tenório, M. B., Dupouy, C., Rodier, M., and Neveux, J.: Trichodesmium and other planktonic cyanobacteria in New Caledonian waters (SW tropical Pacific) during an El Niño episode, Aquatic Microbial Ecology, 81, 219–241, 2018.

van Baalen, C. and Brown, R. M.: The ultrastructure of the marine blue green alga, Trichodesmium erythraeum, with special reference to the cell wall, gas vacuoles, and cylindrical bodies, Archiv für Mikrobiologie, 69, 79–91, https://doi.org/10.1007/BF00408566, 1969.

Villareal, T. A. and Carpenter, E. J.: Buoyancy Regulation and the Potential for Vertical Migration in the Oceanic Cyanobacterium Trichodesmium, Microbial Ecology, 45, 1–10, http://www.jstor.org/stable/4287673, 2003.

Wang, M. and Shi, W.: Estimation of ocean contribution at the MODIS near-infrared wavelengths along the east coast of the U.S.: Two case studies, Geophysical Research Letters, 32, https://doi.org/10.1029/2005GL022917, 2005.

Wang, M. and Shi, W.: The NIR-SWIR combined atmospheric correction approach for MODIS ocean color data processing, Optics Express, 15, 15 722, https://doi.org/10.1364/OE.15.015722, 2007.

Westberry, T. K., Siegel, D. A., and Subramaniam, A.: An improved bio-optical model for the remote sensing of Trichodesmium spp. blooms, Journal of Geophysical Research: Oceans, 110, 1–11, 2005.
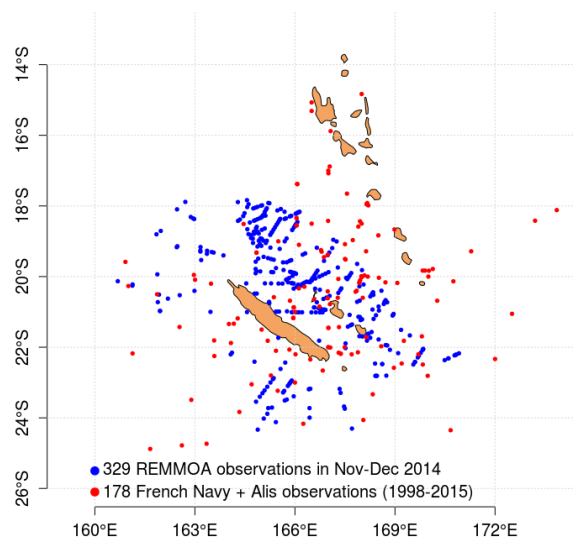
Figure 1. Map of in-situ (visual) observations of *Trichodesmium* mats gathered on the studied region.
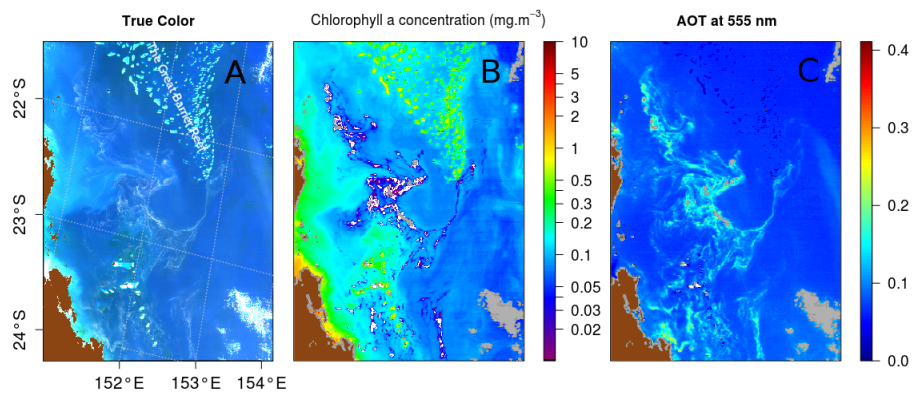
Figure 2. MODIS-Aqua tile A2007290.0355 used in McKinna et al. (2011): (A) RGB image from R_{rc} generated with $R = 645nm$, $G = 555nm$ and $B = 469nm$ computed using the formulae $0.29319407 + 0.45585 \times atan(50 \times (R_{rc}) - 0.015))$; (B) aerosol optical thickness at $555nm$ derived using the NIR atmospheric correction algorithm by Gordon and Wang (1994); (C) Chlorophyll concentration product computed from R_{rs} using OC3 and OCI (Hu et al., 2012). Cloud pixels in grey and land pixels in brown.
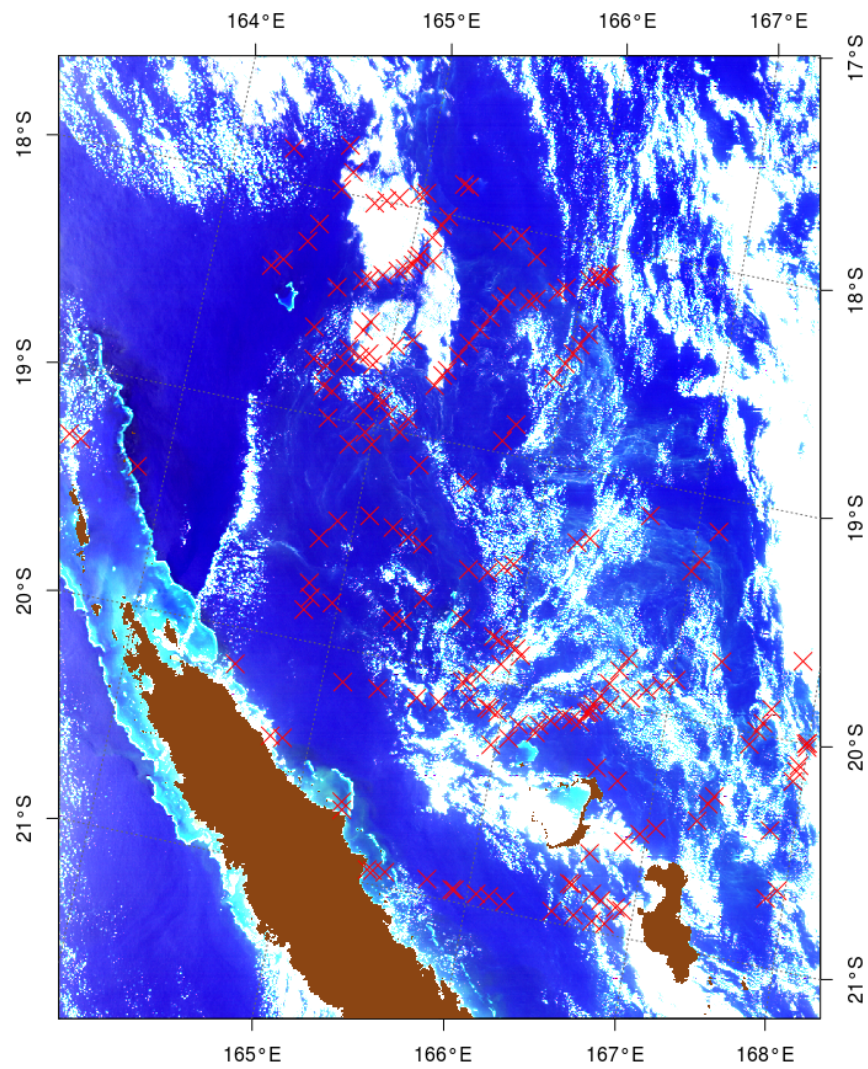
Figure 3. "True color" image of the 17th December "2014A2014351.0255" for which in situ observations (red crosses) exist in the OBT database, and used for the test and adjustment of the different bio-optical algorithms.
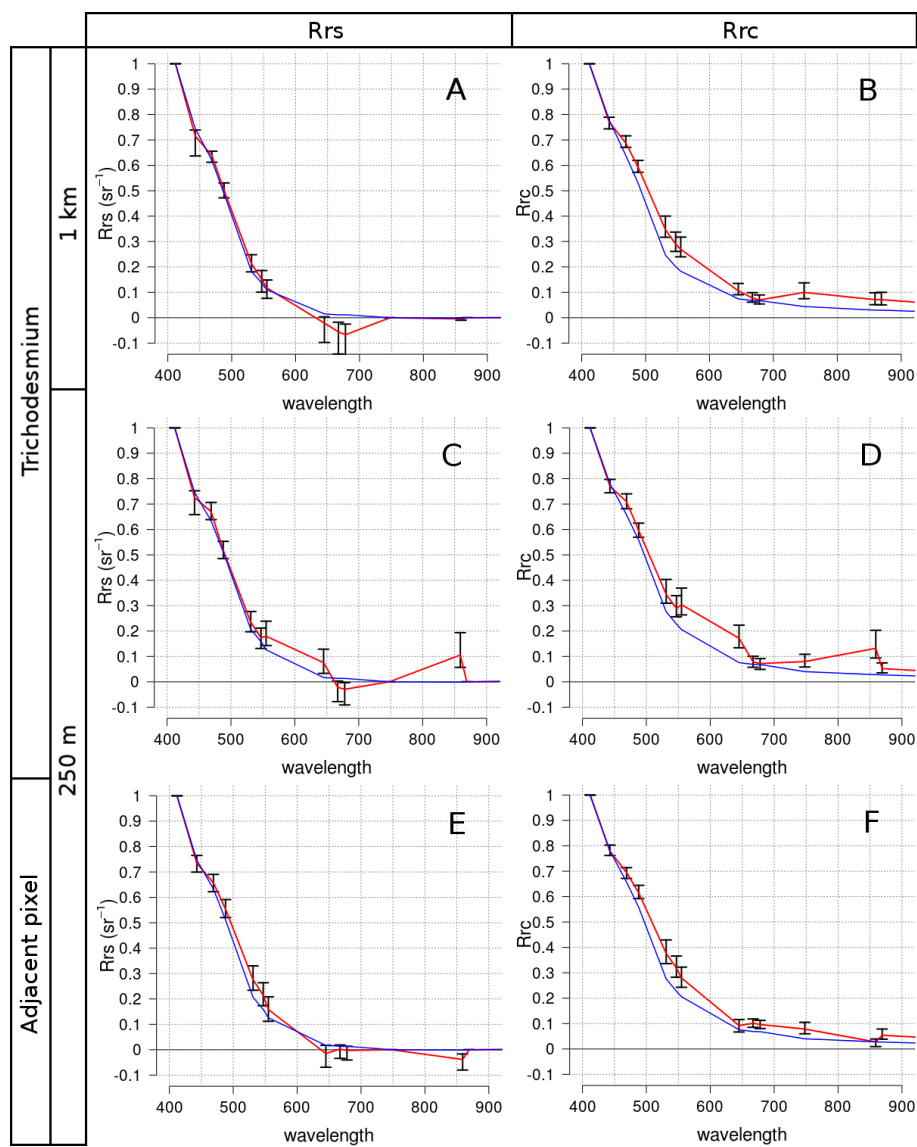
Figure 4. MODIS Spectra of *Trichodesmium* mats (A, B, C and D) and adjacent areas (E and F) normalized by the maximum spectral value of all wavelengths, with pixels resolution at 1 km (A and B) and 250m (C, D, E and F). A, C and E are R_{rs} reflectances. B, D and F are R_{rc} reflectances. Average is red line and error bars are the standard deviation. The average of the water signal is the blue line.
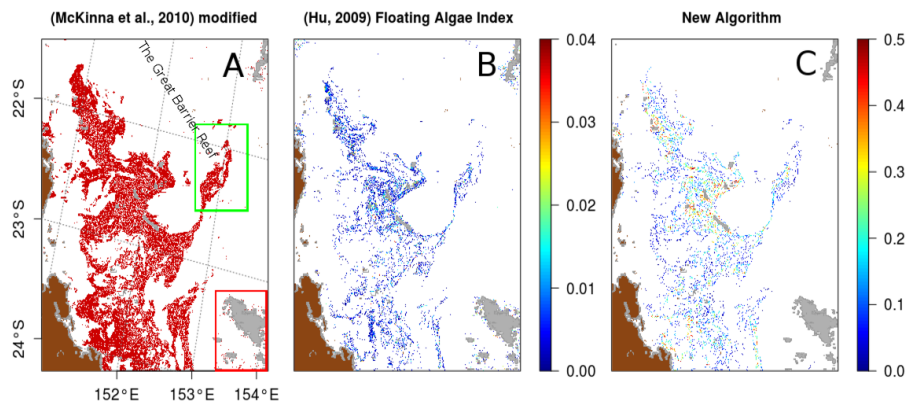
Figure 5. *Trichodesmium* mats detection results on MODIS tile "A2007290.0355": (A) detected pixels with McKinna modified algorithm in red, (B) FAI value of detected pixels with FAI algorithm, (C) pixels detected with the new algorithm, color represents $R_{rs}(678)$ absolute value of the detected pixels. Cloud pixels in grey.
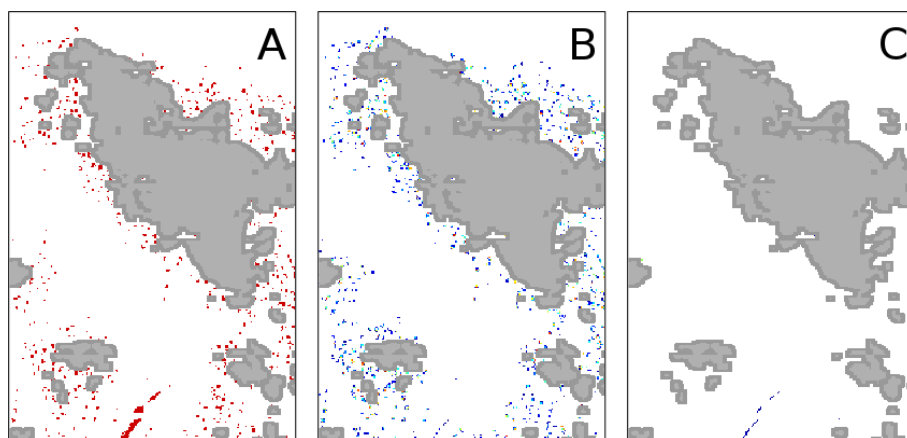
Figure 6. MODIS tile "A2007290.0355" zoomed of the red square area (24°S, Figure 5). Pixels resulting from a false positive detection of (A) the McKinna modified algorithm, (B) FAI and (C) the new algorithm for the area in red on the Figure 5. Cloud pixels in grey.
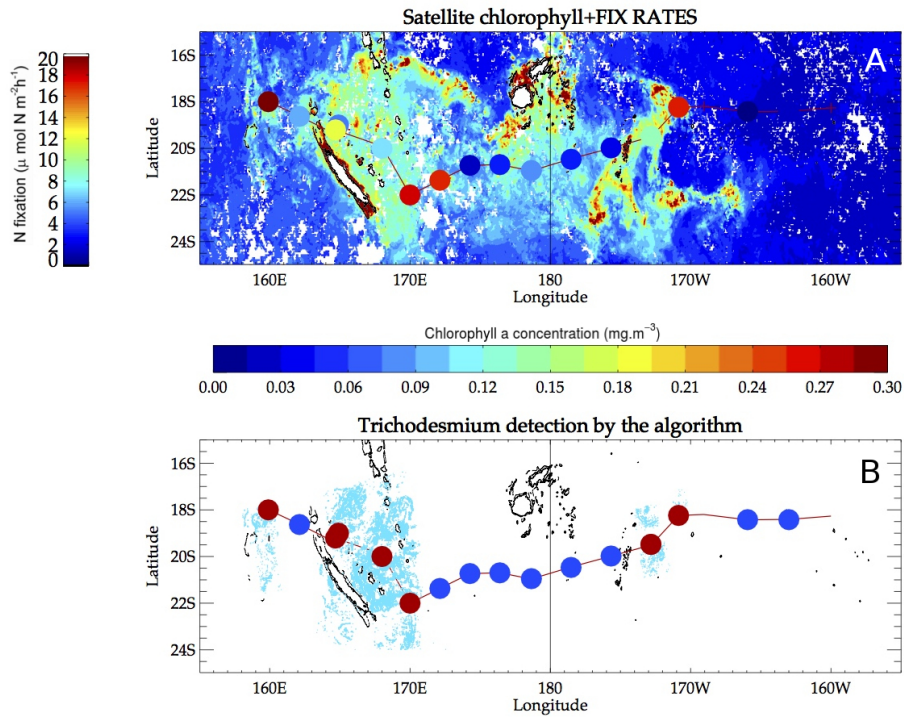
Figure 7. (A) Background is the monthly composite of satellite chlorophyll for March 2015, with the corresponding chlorophyll-a concentrations given by the colorbar underneath the map. Superimposed colored dots are in-situ fixation rates measured on the OUTPACE track with values given by the left colorbar. (B) In the background, cyan pixels are pixels detected as *Trichodesmium* by our algorithm. The colored dots superimposed show the absence (blue) or presence (red) of detected pixels within a radius of 50 km around OUTPACE stations.
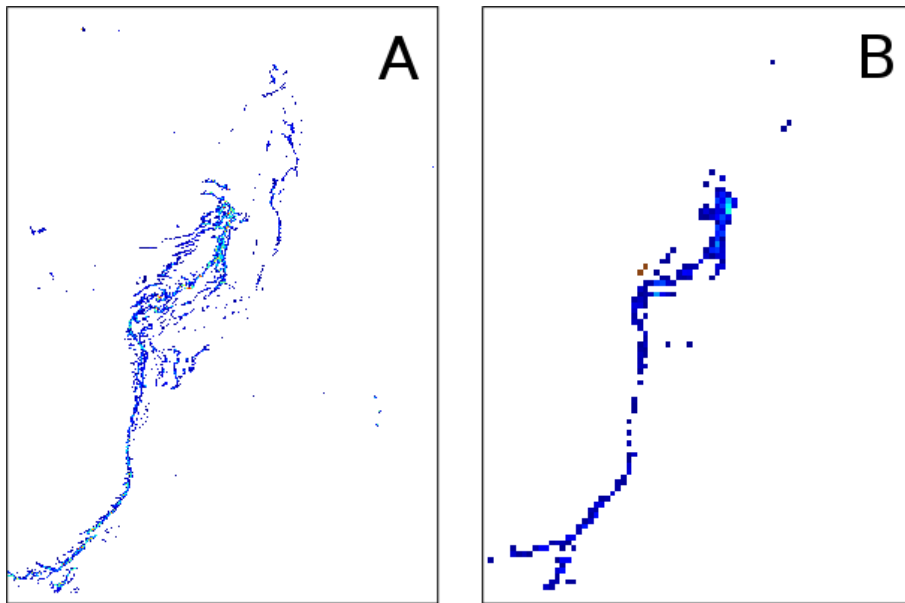
Figure 8. FAI application to the MODIS tile "A2007290.0355": zoomed of the green square area (22.5 °S, Figure 5). (A) Results at 250 m resolution, (B) the same scene at 1 km resolution. Only a few pixels are remaining corresponding to the densest part of the surface mat, showing the loss of detected mats.
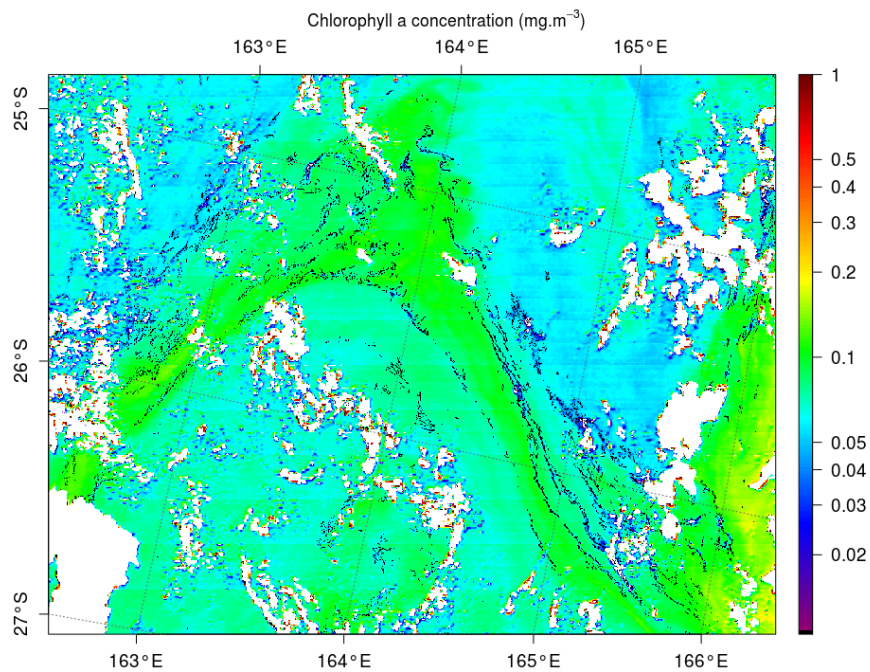
Figure 9. MODIS-Aqua image at 250 m taken on the 6 March 2015 to the south of the OUTPACE cruise illustrating the structure of the chlorophyll (colors) together with the filaments of *Trichodesmium* detected by our algorithm (in black). Cloud pixels in white

Table 1. Specification of the first 13 MODIS channels, including primary use, central wavelength, bandwidth and spatial resolution. http://eoweb.dlr.de:8080/short_ guide/D-MODIS.html

	Central wavelength (nm)	MODIS band number	Spectral coverage and bandwidth (nm)	Spatial resolution (m)	Key use in SeaDAS
Visible	412	8	405 - 420 (15)	1000	Ocean Color, Phytoplancton
	443	9	438 - 448 (10)	1000	Ocean Color, Phytoplancton
	469	3	459 - 479 (20)	500	Land/Vegetation
	488	10	483 - 493 (10)	1000	Ocean Color, Phytoplancton
	531	11	526 - 536 (10)	1000	Ocean Color, Phytoplancton
	547	12	542 - 552 (10)	1000	Ocean Color, Phytoplancton
	555	4	620 - 670 (20)	500	Land/Vegetation
	645	1	662 - 670 (50)	250	Land, Cloud, Aerosol
	667	13	662 - 672 (10)	1000	Ocean Color, Phytoplancton
	678	14	673 - 683 (10)	1000	Chlorophyll Fluorescence
Near infrated	748	15	743 - 753 (10)	1000	Ocean Color, red edge, atmospheric correction
	859	2	841 - 876 (35)	250	Land, Cloud, Aerosol
	869	16	862 - 877 (15)	1000	Ocean Color, red edge, atmospheric correction

Table 2. Satellite image with in-situ observations used to analyze *Trichodesmium* mat and adjacent spectra.

Tiles	Date	Location
A2002341.0255	7 December 2002	East of New Caledonia
A2004047.0230	16 February 2004	Loyalty islands
A2004059.0255	28 February 2004	East of New Caledonia
A2014344.0245	10 December 2014	Loyalty islands (East of Ouvea)
A2014351.0255	17 December 2014	Northeast of New-Caledonia
A2014353.0240	19 December 2014	Between Vanuatu and New-Caledonia